Predictions of neutralino dark matter event rates in minimal supergravity unification

R. Arnowitt
Center for Theoretical Physics, Department of Physics, Texas A&M University, College Station, Texas 77843-4242

Pran Nath
*Department of Physics, Northeastern University, Boston, Massachusetts 02115**
and Institute for Theoretical Physics, University of California, Santa Barbara, California 93106
(Received 13 September 1995)

A detailed analysis of dark matter event rates in minimal supergravity models (MSGM's) is given. It is shown analytically that the lightest neutralino $\widetilde{Z}_1$ is the LSP over almost all of the parameter space, and hence the natural candidate for cold dark matter (CDM). The radiative breaking of SU(2)×U(1) constraints is shown to be crucial in determining the expected event rates. Approximate analytic formulas are obtained to determine the gaugino-Higgsino content of the $\widetilde{Z}_1$ particle. From this one can deduce the behavior of the event rates as one varies the SUSY soft breaking parameters and $\tan\beta$. The constraint on the event rates due to the recently measured $b\to s+\gamma$ decay is calculated. It is seen that these data eliminate most of the parameter space where μ (the Higgs mixing parameter) and A_t (the t-quark cubic soft breaking parameter) have the same sign. Since the t quark is close to its Landau pole, A_t is restricted to be mostly positive, and so most of the $\mu>0$ part of the parameter space is eliminated. However, for $\mu<0$, one finds large regions of parameter space where the event rate is large and exceeds 0.01 events/kg day. The importance of proper treatment of the s-channel Z and Higgs poles in calculating the relic density is stressed. The implications of the recent new experiments (SMC and E143) on the quark polarizabilities are analyzed and it is seen that uncertainties in these generally produce only small uncertainties in the event rates. A discussion is also given of the sensitivity of the expected event rates to changes in the allowed range of $\widetilde{Z}_1$ relic density. [S0556-2821(96)05313-1]

PACS number(s): 19.80.Ly, 12.10.Dm, 95.35.+d

I. INTRODUCTION

The nature of the dark matter (DM) which makes up more than 90% of the matter of the universe is a particularly important issue as it may have a fundamental impact both on astronomy and particle physics. Dark matter has currently only been detected by its gravitational interactions, and thus, may be composed of several constituents, e.g., baryonic dark matter (BDM), hot dark matter (HDM), and cold dark matter (CDM) (where ''hot'' and ''cold'' refer to whether the particle was relativistic or nonrelativistic at the time of galaxy formation). One may measure the amount of each species of dark matter by the ratio $\Omega_i=\rho_i/\rho_c$ where ρ_i is the mass density of the ith constituent and $\rho_c=3H^2/8\pi G_N$ is the critical mass density (H is the Hubble constant and G_N is the Newtonian gravitational constant). Within the framework of the inflationary scenario one has $\Sigma\Omega_i=1$. The amount of baryonic matter is severely limited in the big bang cosmology by the observed abundancies of light elements, i.e., $\Omega_B\lesssim 0.1$.

Rotation curves of stars imply a density of dark matter in our Galaxy of

$$\rho_{\rm DM}\cong 0.3\ \ {\rm GeV/cm}^3 \tag{1}$$

and this matter will be impinging on the Earth with velocity $v_{\rm DM}\simeq 320$ km/s. The fact that microlensing finds far more massive compact halo objects (MACHO's) in the direction of galactic center than in the halo of the Galaxy implies that at most 30% of the halo dark matter is made up of MACHO'S [1]. Thus most of the halo of the Galaxy must be cold dark matter, and it is this dark matter that terrestial detectors can observe.

A possible source of hot dark matter is massive neutrinos. In this paper we assume that the cold dark matter component is the lightest supersymmetry neutralino, the $\widetilde{Z}_1$ particle. The anisotropy power spectrum [including the recent Cosmic Background Explorer (COBE) data] puts constraints on the relative amounts of HDM and CDM. A reasonable fit to the full spectrum gives $\Omega_{\rm CDM}:\Omega_{\rm HDM}=2:1$. Assuming $\Omega_B\simeq 0.1$ one then estimates $\Omega_{\widetilde{Z}_1}=0.6$. What is theoretically calculable is Ωh^2 where $h=[H/(100\ {\rm km/s\ Mpc})]$. Current astronomical measurements yield

$$0.4\lesssim h\lesssim 0.8; \tag{2}$$

i.e., two groups of measurements of h exist, one clustering at the lower bound and one at the upper bound. [The inflationary scenario (with zero cosmological constant) requires $h\simeq 0.5$.] Thus we estimate

$$0.1\lesssim \Omega_{\widetilde{Z}_1} h^2\lesssim 0.4 \tag{3}$$

and we will assume these bounds in the following. [Our results are not qualitatively sensitive to the precise upper and lower limits of Eq. (3) and we will discuss below what changes occur if one perturbs them.] We also note that it has recently been suggested [2] that if the value $h\simeq 0.8$ is correct, the age of the universe and other cosmological problems

*Permanent address.

could be accounted for by a cosmological constant with $\Omega \simeq 0.6$–0.8, and the remainder being CDM. This would also lead to $\Omega_{\tilde{Z}_1} h^2$ being in the range of Eq. (3).

Current dark matter detectors plan to obtain a sensitivity of $R \simeq 0.1$ events/kg day. Future developments may improve this to $R = 0.01$ events/kg day. We will thus limit our discussion here to the part of the parameter space where

$$R \gtrsim 0.01 \text{ events/kg day}, \tag{4}$$

since this sensitivity is what one may expect over the next 5–10 yr. Detection of the $\tilde{Z}_1$ depends on their scattering cross section by quarks in the nuclei of the detector. Thus a calculation of event rates depends on two things: (i) that the relic density of $\tilde{Z}_1$ obey the bounds of Eq. (3), which limits the allowed supersymmetric (SUSY) parameter space, and (ii) a calculation of the $\tilde{Z}_1 - q$ cross section. We consider these calculations in this paper within the framework of supergravity grand unification models [3]. While this model is not a complete theory it possesses a sufficient number of accomplishments to warrant using it as the dynamical framework. Thus it accounts naturally for grand unification at a scale $M_G \simeq 10^{16}$ GeV implied by the measurements at the CERN e^+e^- collider LEP of α_1, α_2, and α_3 at M_Z; it allows a natural breaking of supersymmetry (in the hidden sector) at the grand unified theory (GUT) scale (something that cannot be done in a phenomenologically acceptable way in the minimal supersymmetric standard model (MSSM), and is yet to be demonstrated to occur in string theory); it can account for the suppression of flavor-changing neutral current (FCNC) interactions in a natural way; in the minimal supergravity model (MSGM) it depends on only four additional parameters and one sign to describe all the masses and interactions of the 32 new SUSY particles. (This may be compared with 110 new parameters that can occur in the MSSM.)

The supergravity interactions of the MSGM produce four supersymmetry soft breaking terms at M_G scaled by m_0 (universal spin-zero mass), $m_{1/2}$ (universal gaugino mass), and A_0 and B_0 (cubic and quadratic soft breaking constants). One of the remarkable features of this theory is that this spontaneous breaking of supersymmetry at M_G generates, by radiative renormalization group (RG) corrections, the breaking of $SU(2) \times U(1)$ at the electroweak scale [4]: supersymmetry breaking produces $SU(2) \times U(1)$ breaking. We will see below that radiative breaking is a key element in the analysis of dark matter event rates, and failure to include it loses much of the predictive power of the theory.

While the MSGM possesses only four additional parameters to describe SUSY phenomena, and this is far fewer than the 20 to 30 of the 110 possible new parameters that is commonly assumed in the MSSM, it still possesses a large parameter space. (Ideally, one would like to have four experiments to determine the four parameters, making all further predictions of the theory unique.) Recently, however, there have been two new pieces of data, the CLEO measurement of the $b \to s + \gamma$ branching ratio [5] and the Collider Detector at Fermilab (CDF) and D0 measurements of the top quark mass [6]. We will see below that, while large error flags still remain in these data, they greatly reduce the allowed parameter space.

There has been considerable activity in the recent past to calculate expected event rates for dark matter detectors [7–13]. However, Refs. [7–9] do not impose radiative breaking and thus can get abnormally high event rates (often by choosing the PC odd Higgs boson to be too light). The major part of the analysis of Ref. [10] is also done in this framework, and when radiative breaking is introduced the entire parameter space is not scanned. Thus Ref. [10] predicts event rates that are too low. The analyses [7–11] also impose relic density constraints which leave out the full thermal averaging over the Z and h (light Higgs boson) s-channel poles. It is known that such omissions can generate serious errors in density calculations [14,15], and we will see below that it is important to treat s-channel poles correctly for about one-half the parameter space. Finally Refs. [7,8] do not include the heavy Higgs boson, H, in the event rate calculation, the importance of which was first pointed out in Ref. [16].

The plan of this paper is the following. In Sec. II we briefly review the ideas of radiative electroweak breaking and discuss the origin of the scaling relations between the masses of the light neutralinos and charginos and the gluino. In Sec. III we exhibit an approximate analytic formula for the gaugino and Higgsino content of the $\tilde{Z}_1$ in the scaling regime. In Sec. IV we discuss the relic density calculation, exhibit the importance of correct treatment of the s-channel resonances, and also discuss the event rate calculations. We also show that uncertainties in the nucleon spin content do not have any significant effect on event rates for all targets except for the lightest ones such as ^{3}He and CaF_2. These results are in contrast with a recent analysis [17] where the coherent part of the scattering was ignored and hence claimed a large effect. Section V is concerned with constraints on event rates and SUSY parameter space due to the $b \to s + \gamma$ decay and the top quark mass. We show there that there are sizable regions of the parameter space with $R > 0.01$ including this constraint, and thus our results differ from those of Ref. [18] which concludes that with the $b \to s + \gamma$ constraint, the event rate R is very small. We discuss in Sec. VI the effect of varying the endpoints of Eq. (3). Section VII gives the conclusions. The MSGM predicts that the $\tilde{Z}_1$ is the lightest supersymmetric particle over almost all the parameter space. The analytic analysis of this is given in the Appendix.

II. RADIATIVE ELECTROWEAK BREAKING

At the GUT scale the MSGM can be described by the superpotential

$$W = \mu_0 H_1 H_2 + W_Y + \frac{1}{M_G} W^{(4)}, \tag{5}$$

where W_Y is the cubic Yukawa couplings and $W^{(4)}$ contains any quartic nonrenormalizable couplings (which possibly lead to proton decay). The spontaneous breaking of supersymmetry leads to the soft supersymmetry breaking effective potential $V_{\rm SB}$ and gaugino mass term $L^{\lambda}_{\rm mass}$:

$$V_{\rm SB} = m_0^2 \sum_a z_s^+ z_a + (A_0 W_Y + B_0 \mu_0 H_1 H_2 + \text{H.c.}), \tag{6}$$

$$L^{\lambda}_{\rm mass} = -m_{1/2}\bar{\lambda}^{\alpha}\lambda^{\alpha}, \tag{7}$$

where $\{z_a\}$ are the scalar fields and λ^α the gaugino fields. Equations (5)–(7) arise after the supergravity interactions cause the spontaneous breaking of supersymmetry in the hidden sector, the GUT interactions cause the breaking of the GUT group G to SU(3)×SU(2)×U(1), all superheavy and hidden sector fields are integrated out, and nonrenormalizable terms scaled by $(1/M_{\rm Pl})$ are neglected. The universality of the soft breaking parameters, m_0, A_0, B_0, and $m_{1/2}$, is a consequence of the universality of gravitational couplings, plus the additional assumption that the hidden sector fields in the Kahler potential also couple universally to the physical fields. (This universality also guarantees suppression of FCNC interactions and thus is phenomenologically desirable.) The above results are generally insensitive to the nature of the GUT group provided the representations used to break G are not too large (so that GUT threshold corrections are not too big).

The effective potential may be reduced to the electroweak scale by using the renormalization group (RG) equations. Minimizing the Higgs potential with respect to $\langle H_{1,2}\rangle$ yields [4]

$$\mu^2 = \frac{\mu_1^2 - \mu_2^2\tan^2\beta}{\tan^2\beta - 1} - \frac{1}{2}M_Z^2, \quad \sin 2\beta = \frac{-2B\mu}{2\mu^2 + \mu_1^2 + \mu_2^2}. \tag{8}$$

Here $\mu_i^2 = m_{H_i}^2 + \Sigma_i$ where $m_{H_i}^2$ is the running H_i mass at scale $Q \approx M_Z$ and Σ_i are loop corrections. The $m_{H_i}^2$ are given by

$$m_{H_1}^2 = m_0^2 + m_{1/2}^2 g(t), \tag{9}$$

$$m_{H_2}^2 = m_{1/2}^2 e(t) + A_0 m_{1/2} f(t) + m_0^2 h(t) - k(t)A_0^2, \tag{10}$$

where the form factors e,f,g,h,k are defined in Ibañez *et al.* [4], the gluino mass is $m_{\tilde g} = (\alpha_3/\alpha_G)m_{1/2}$ (with α_G the GUT coupling constant), and $t = \ln(M_G^2/Q^2)$. One may show that solutions exist to Eqs. (8), i.e., that SU(2)×U(1) is spontaneously broken, if and only if at least one of the supersymmetry soft breaking interactions are nonzero. Thus it is the supergravity interactions at M_G that give rise to the breaking of SU(2)×U(1) at the electroweak scale.

To obtain a qualitative picture of the implications of electroweak breaking, one notes from Eq. (8) that for $\tan^2\beta \gg 1$ (i.e., $\tan\beta \gtrsim 2$–3) that

$$\mu^2 \simeq -m_{H_2}^2 - \frac{1}{2}M_Z^2 - \Sigma_2. \tag{11}$$

Thus for electroweak breaking to occur, it is necessary for $m_{H_2}^2$ to turn negative. (Σ_2 is generally a small correction.) The measured value of the top quark mass is $m_t = (176 \pm 8 \pm 10)$ GeV from CDF [6] and $m_t = (199^{+19}_{-21} \pm 22)$ GeV from D0 [6] while indirect determinations from LEP yield $m_t = 164^{9}_{-10}{}^{6}_{-4}$ GeV [19]. These imply that the top is relatively close to its Landau pole. In this domain, for Q at the electroweak scale, $h(t)$, $e(t)$, and $f(t)$ are negative and $g(t)$ and $k(t)$ are positive. Further, both $|h|$ and $|e|$ are of order 1. (For a detailed discussion of the effects of the Landau pole see Ref. [20].) Thus $m_{H_2}^2$ does indeed turn negative allowing SU(2)×U(1) breaking to occur at the electroweak scale.

In the following we will restrict m_0 and $m_{\tilde g}$ to be less than 1 TeV to prevent an unreasonable amount of fine tuning. [Actually we will see that Eq. (4) implies $m_{\tilde g} \lesssim (650$–$700)$ GeV.] Equation (11) then implies

$$\mu^2 \gg M_Z^2. \tag{12}$$

[which is satisfied if $\mu \gtrsim (2$–$3)M_Z$] for almost the entire parameter space. Note also that the above discussion implies that μ^2 is an increasing function of $m_{\tilde g}^2$ and m_0^2.

Equation (12) is essentially the remnants of the gauge hierarchy problem in supersymmetry, i.e., from Eqs. (9)–(11), μ is scaled by m_0 and $m_{\tilde g}$ and we allow the latter to go as high as 1 TeV. It has been previously shown [21] that Eq. (12) leads to a set of scaling relations between the light neutralinos, chargino, and gluino,

$$2m_{\tilde Z_1} \cong m_{\tilde Z_2} \cong m_{\tilde W_1} \simeq \left(\frac{1}{3} - \frac{1}{4}\right)m_{\tilde g} \tag{13}$$

as well as the additional relations

$$m_{\tilde Z_{3,4}} \cong m_{\tilde W_2} \gg m_{\tilde Z_1}; \quad m_H \cong m_{H^\pm} \cong m_A \gg m_h. \tag{14}$$

Also one finds

$$63\ \text{GeV} \lesssim m_h \lesssim 120\ \text{GeV}, \tag{15}$$

where the lower bound on m_h is the current LEP limit. Equations (12)–(14) are thus a direct consequence of radiative electroweak breaking, and we will see below that they play a dominant role in determining relic densities and dark matter detection rates.

III. COMPOSITION OF $\tilde Z_1$

The $\tilde Z_1$ is generally a mixture of gauginos $\tilde W_3$, $\tilde B$ and Higgsinos $\tilde H_1$, $\tilde H_2$. We write

$$\tilde Z_1 = n_1\tilde W_3 + n_2\tilde B + n_3\tilde H_1 + n_4\tilde H_2. \tag{16}$$

The expansion coefficients n_i are determined by diagonalizing the neutralino mass matrix. In the $(\tilde W_3, \tilde B, \tilde H_1, \tilde H_2)$ basis this reads [3]

$$M_{\tilde Z} = \begin{pmatrix} \tilde m_2 & 0 & a & b \\ 0 & \tilde m_1 & c & d \\ a & c & 0 & -\mu \\ b & d & -\mu & 0 \end{pmatrix}, \tag{17}$$

where $\tilde m_i = (\alpha_i/\alpha_3)m_{\tilde g}$, $a = M_Z\cos\theta_w\cos\beta$, $b = -M_Z\cos\theta_w\sin\beta$, $c = -M_Z\sin\theta_w\cos\beta$, and $d = M_Z\sin\theta_W\sin\beta$. The $\tilde Z_1$ is the lowest mass eigenvector of $M_{\tilde Z}$, which may be determined in general numerically. However, as discussed in Sec. II, radiative breaking implies $\mu^2 \gg M_Z^2$. One may generate an approximate analytic form by treating the two blocks proportional to M_Z perturbatively. To second order perturbation theory one finds

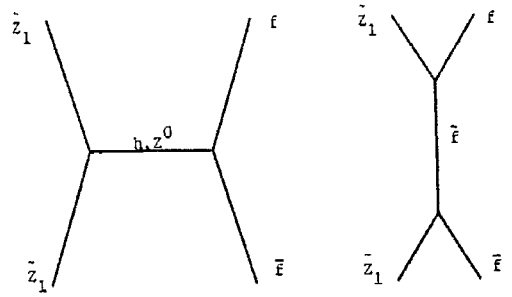

FIG. 1. $\widetilde{Z}_1$ annihilation diagrams for annihilation in the early universe.

$$n_1 \cong -\frac{1}{2}\frac{M_Z}{\mu}\frac{1}{(1-\widetilde{m}_1^2/\mu^2)}\frac{M_Z}{\widetilde{m}_2-\widetilde{m}_1}\sin 2\theta_W\left[\sin 2\beta+\frac{\widetilde{m}_1}{\mu}\right], \tag{18}$$

$$n_2 = 1-\frac{1}{2}\frac{M_Z^2}{\mu^2}\frac{1}{(1-\widetilde{m}_1^2/\mu^2)^2}\sin^2\theta_W\left[1+\frac{\widetilde{m}_1}{\mu}\sin 2\beta+\frac{\widetilde{m}_1^2}{\mu^2}\right], \tag{19}$$

$$n_3 = \frac{M_Z}{\mu}\frac{1}{1-\widetilde{m}_1^2/\mu^2}\sin\theta_W\sin\beta\left[1+\frac{\widetilde{m}_1}{\mu}\cot\beta\right], \tag{20}$$

$$n_4 = -\frac{M_Z}{\mu}\frac{1}{1-\widetilde{m}_1^2/\mu^2}\sin\theta_W\cos\beta\left[1+\frac{\widetilde{m}_1}{\mu}\tan\beta\right]. \tag{21}$$

Equations (18)–(21) differ from the numerical computer results by amounts $\delta n_i \lesssim 0.03$ over almost the entire parameter space (and are generally a good deal better). Thus one may use them to understand the nature of the solutions. One sees first that the $\widetilde{Z}_1$ is mostly bino since n_2 deviates from unity by second order effects, $O(M_Z^2/\mu^2)$. Usually, $n_2 > 0.95$ and often larger. However, n_3, n_4, and n_1 are first order, $O(M_Z/\mu)$. This allows the Higgsino components of the $\widetilde{Z}_1$ to become considerable, e.g., $n_3 \approx 0.2$. The coherent part of the $\widetilde{Z}_1$-nucleus scattering in dark matter detectors, depend upon the interference between the gaugino and Higgsino components of the $\widetilde{Z}_1$ [7]. Thus such terms can become quite large, and as will be discussed in Sec. IV, this means that the coherent scattering almost always dominates the incoherent (spin dependent) scattering. Thus there is a large difference between a $\widetilde{Z}_1$ whose bino amplitude is 0.95 and one which is 100% bino, and one cannot approximate the former as being pure bino. We also note that the above results are a direct consequence of the radiative breaking conditions, and would not in general hold without them.

IV. RELIC DENSITY AND EVENT RATE ANALYSIS

The primordial $\widetilde{Z}_1$, created at the time of the big bang, can annihilate in the early universe. The main diagrams for this are shown in Fig. 1 [22]. At high temperature, the $\widetilde{Z}_1$ is in thermal equilibrium with its decay products. However, when the annihilation rate falls below the expansion rate of the universe, freeze out occurs at temperature T_f. The $\widetilde{Z}_1$ are then disconnected from the background and continue to annihilate. In the simplest approximation [23] (accurate to about $\pm 25\%$) the current relic density is given by

$$\Omega_{\widetilde{Z}_1} h^2 \cong 2.5\times 10^{-11}\left(\frac{T_{\widetilde{Z}_1}}{T_\gamma}\right)^3\left(\frac{T_\gamma}{2.75}\right)^3\frac{(N_f)^{1/2}}{J(x_f)}, \tag{22}$$

where

$$J(x_f) = \int_0^{x_f} dx\langle\sigma v\rangle, \quad x_f = kT_f/m_{\widetilde{Z}_1}. \tag{23}$$

Here $x = kT/m_{\widetilde{Z}_1}$, N_f is the effective number of degrees of freedom at freeze out, $(T_{\widetilde{Z}_1}/T_\gamma)^3$ is the reheating factor, and T_γ the current microwave radiation temperature (in K). In Eq. (23), σ is the annihilation cross section, v is the relative velocity and angular brackets means thermal average.

Freeze out generally occurs when the $\widetilde{Z}_1$ are nonrelativistic, i.e., at $x_f = kT_f/m_{\widetilde{Z}_1} \simeq 1/20$. Thus the thermal average may be taken over a Boltzmann distribution:

$$\langle\sigma v\rangle = \int_0^\infty dv\ v^2\sigma v\ \exp[-v^2/4x] \Big/ \int_0^\infty dv\ v^2 \times \exp[-v^2/4x]. \tag{24}$$

The nonrelativistic nature of the annihilation process has lead, in the past, to making a nonrelativistic expansion of σv i.e., $\sigma v \cong a + b(v^2/c^2) + \cdots$; after which the thermal average becomes trivial to take. This is a good approximation for the t-channel pole diagrams of Fig. 1, and for the s-channel diagrams when $2m_{\widetilde{Z}_1}$ is not in the vicinity of the h or Z poles. However, when $2m_{\widetilde{Z}_1}$ is near the s-channel poles, the nonrelativistic approximation fails [14] and can produce errors as large a factor of 100 [15] due to the fact that σv is a rapidly varying function in this region. Further, the thermal averaging smears the region where this effect can occur (characteristically over a region $\approx$10 GeV in $m_{\widetilde{Z}_1}$ or $\approx$50 GeV in $m_{\widetilde{g}}$). For this situation one can first perform the integral of Eq. (24) analytically, and then calculate Eq. (23) numerically.

In the following, we will investigate the parameter space defined by the bounds

$$100\ \text{GeV} \leqslant m_0 \leqslant 1\ \text{TeV}; \quad 150\ \text{GeV} \leqslant m_{\widetilde{g}} \leqslant 1\ \text{TeV}, \tag{25}$$

$$-6 \leqslant A_t/m_0 \leqslant 6; \quad 2 \leqslant \tan\beta \leqslant 20. \tag{26}$$

The lower bound on $m_{\widetilde{g}}$ is the current Tevatron bound and the upper bounds on m_0, $m_{\widetilde{g}}$ are to prevent excessive fine tuning of parameters. [Similarly, we view $\tan\beta \gtrsim 30$ a fine-tuning of the Higgs vacuum expectation value (VEV) ratio.] The range on A_t covers the allowed parameter space (when all other experimental constraints are imposed). One may estimate the region of this parameter space where the above discussion of s-channel poles is important. The scaling relations, Eqs. (13) and (14), allow us to choose $m_{\widetilde{g}}$ as the independent variable. One sees from these relations, that, varying over the field parameter space, one is generally near an s-channel resonance (h or Z pole) when $m_{\widetilde{g}} \lesssim 450$ GeV, and hence for this region one must treat the s-channel terms accurately. This is borne out by detailed numerical calculations

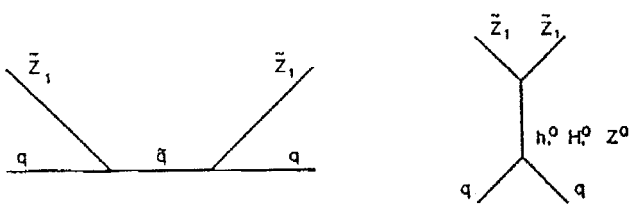

FIG. 2. $\tilde{Z}_1$-quark scattering diagrams for a terrestial dark matter detector.

which show that significant errors occur in the calculation of $\Omega_{\tilde{Z}_1}h^2$ with $m_{\tilde{g}} \lesssim 450$ GeV when the nonrelativistic approximation to $\langle \sigma v \rangle$ is made, while the approximation is generally good for $m_{\tilde{g}} > 450$ GeV. Since the constraint on detection rate, $R \geq 0.01$ events/kg day, requires $m_{\tilde{g}} \lesssim (650-700)$ GeV, we see that a correct treatment of the s-channel poles is important for a large fraction of the total parameter space.

Detection of dark matter impinging on the Earth depends upon the $\tilde{Z}_1$-quark scattering cross section for the quarks in the nuclei of the detector. The basic diagrams are shown in Fig. 2. This process has been studied by a number of authors [24], and can be represented by the effective Lagrangian

$$L_{\text{eff}} = (\overline{\chi_1}\gamma^\mu\gamma^5\chi_1)[\overline{q}\gamma_\mu(A_q P_L + B_q P_R)q] + (\overline{\chi_1}\chi_1)(\overline{q}C_q m_q q). \tag{27}$$

Here χ_1 is the $\tilde{Z}_1$ field, q is the quark field, and $P_{R,L} = (1 \pm \gamma^5)/2$. The coefficients A_q and B_q arise from the Z t-channel pole and the $\tilde{q}$ s-channel pole, while C_q comes from the h^0 and H^0 t-channel poles and the $\tilde{q}$ s-channel pole. (We follow the notation of Ellis and Flores [7] where explicit formulas for A_q, B_q, C_q are given for the $\tilde{q}$, h, and Z pole diagrams.)

The first term of Eq. (27) gives rise to spin dependent (incoherent) scattering while the second term gives rise to spin independent (coherent) scattering. Summing over all the quarks in the nucleus, the latter term then produces an additional factor of the nuclear mass, M_N. The event rate for a detector then takes the form [24]

$$R = [R_{\text{SI}} + R_{\text{SD}}]\left[\frac{\rho_{\tilde{Z}_1}}{0.3 \text{ GeV cm}^{-3}}\right]\left[\frac{v_{\tilde{Z}_1}}{320 \text{ km/s}}\right]\frac{\text{events}}{\text{kg day}}, \tag{28}$$

where $\rho_{\tilde{Z}_1}$ is the local mass density of $\tilde{Z}_1$, $v_{\tilde{Z}_1}$ the incident $\tilde{Z}_1$ velocity, and the spin independent (SI) and spin dependent (SD) rates have the form [25]

$$R_{\text{SI}} = \frac{16 m_{\tilde{Z}_1} M_N^3 M_Z^4}{[M_N + m_{\tilde{Z}_1}]^2}|A_{\text{SI}}|^2, \tag{29}$$

$$R_{\text{SD}} = \frac{16 m_{\tilde{Z}_1} M_N}{[M_N + m_{\tilde{Z}_1}]^2}\lambda^2 J(J+1)|A_{\text{SD}}|^2, \tag{30}$$

where J is the nuclear spin and λ is defined by $\langle N|\Sigma \mathbf{S}_i|N\rangle = \lambda\langle N|\mathbf{J}|N\rangle$. We note that for large M_N, $R_{\text{SI}} \sim M_N$ while $R_{\text{SD}} \sim 1/M_N$, showing that the heavy nuclei are best for detectors sensitive to spin independent scattering.

Since the squarks are generally heavy over most of the parameter space, A_{SI} is dominated by its Higgs contributions which has the general form [26]

$$A_{\text{SI}}^{\text{Higgs}} \sim \frac{g_2^2}{4M_W}\left[\frac{F_h}{m_h^2}\begin{Bmatrix}\dfrac{\cos\alpha_H}{\sin\beta} \\ \dfrac{-\sin\alpha_H}{\cos\beta}\end{Bmatrix} + \frac{F_H}{m_H^2}\begin{Bmatrix}\dfrac{\sin\alpha_H}{\sin\beta} \\ \dfrac{\cos\alpha_H}{\cos\beta}\end{Bmatrix}\right]\begin{matrix} u & \text{quark} \\ d & \text{quark'}\end{matrix} \tag{31}$$

where $F_h = (n_1 - n_2\tan\theta_W)(n_4\cos\alpha_H + n_3\sin\alpha_H)$ and $F_H = (n_1 - n_2\tan\theta_W)(n_4\sin\alpha_H - n_3\cos\alpha_H)$ and α_H is the rotation angle needed to diagonalize the $h - H^0$ mass matrix. Thus the SI scattering arises from interference between the gaugino and Higgsino parts of the $\tilde{Z}_1$, i.e., from Eqs. (18)–(21) from the $n_2 \times n_3$ terms of $F_{h,H}$ for most of the parameter space. In general (including the loop corrections to the Higgs mass matrix [27]) one finds that $\tan\alpha_H \approx 0.1$. Hence, for most of the parameter space, the h contribution to d-quark scattering is suppressed by a factor of $\tan^2\alpha_H$ relative to the H, and this can overcome the fact that $m_H{}^2/m_h{}^2 \gg 1$. In fact we find that the H contribution varies from 1/10 to 10 times the h contribution as one varies over the full parameter space, and it is essential to keep both neutral CP even Higgs bosons in the analysis [16].

In contrast to the above, the contributions to A_{SD} from the Z pole depends on $n_3^2 - n_4^2$ which is small by Eqs. (18)–(21). Thus for heavy nuclei detectors one always has

$$R_{\text{SI}} \gg R_{\text{SD}} \tag{32}$$

and even for the light CaF_2 detector which has a large $\lambda^2 J(J+1)$ value, the spin independent scattering dominates over most of the parameter space.

R_{SD} depends on the spin content of the nucleons defined by

$$\langle n|\overline{q}\gamma^\mu\gamma^5 q|n\rangle = 2 s_{(n)}^\mu \Delta q, \tag{33}$$

where $s_{(n)}^\mu$ is the spin four-vector of nucleon n, and Δq measures the part of the nucleon spin carried by quark q. It has been suggested [17] that the differences between older data [28] and more recent data [29] determinations of Δq (particularly Δs) could produce uncertainties in the value of R leading to errors as large as a factor of 30. This could indeed be the case if the Z_1 was pure gaugino (i.e., $n_2 = 1$, $n_3 = n_4 = n_1 = 0$) for then R_{SI} would vanish. However, as we saw above, a significant interference between the gaugino and Higgsino parts of the $\tilde{Z}_1$ exists (i.e., the $\tilde{Z}_1$ amplitude has a gaugino amplitude of only about 0.95) leading instead to Eq. (32) for heavy nuclei, minimizing the effect. Figure 3 shows the ratio between the predicted value of the total R using the new and old data for Δq for a Ge detector. The difference is less than 10% over the entire parameter space. While larger errors can exist for a CaF_2 detector, where R_{SD} is large, even here the difference is less than $\pm 30\%$ over 92% of the parameter space.

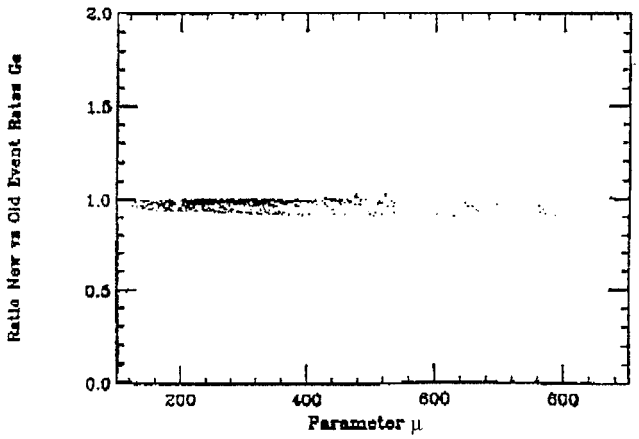

FIG. 3. R(new)/R(old) vs μ for a Ge detector. ''New'' data is Ref. [29] and ''old'' data Ref. [28].

A more serious uncertainty exists in $R_{\rm SI}$ due to a lack of knowledge of the s-quark content of a nucleon defined by $\langle n|m_s\overline{ss}|n\rangle \equiv f_s M_n$. Estimates of f_s [30] have about a 50% uncertainty leading to a $\pm(30-50)$% uncertainty in $R_{\rm SI}$. This will not, however, change the qualitative nature of the results given below.

One may now understand analytically the dependence of the event rate on the different SUSY parameters. From Eq. (11), we see that μ^2 is an increasing function of $-m_{H_2}^2$ and hence by Eq. (10) an increasing function of $m_{\tilde{g}}$. As shown in the discussion following Eq. (31), the major contribution to $A_{\rm SI}$ (which dominates the total event rate R) is proportional to $(n_2 n_3)$ [or $(n_2 n_4)$] which by Eqs. (18)–(21) are the leading $[Q(M_z/\mu)]$ terms. These decrease with increasing μ. Thus one expects R to be a decreasing function of $m_{\tilde{g}}$. This indeed was what was seen in the detailed computer calculations of Ref. [12]. Further, for radiative breaking, which implies $\tan\beta > 1$, Eq. (31) also shows that the d-quark amplitude is an increasing function of $\tan\beta$. Again the computer calculations of Ref. [12] show this rapid rise of R with $\tan\beta$. The behavior of R with respect to m_0 is more complicated. It turns out that there is an accidental cancellation of the coefficient of m_0^2 in Eq. (10) at $m_t \sim 170$ GeV. Above this the coefficient turns negative causing μ to increase at fixed A_t with increasing m_0.

The calculation of the detector event rates now proceeds as follows. One calculates $\Omega_{\tilde{Z}_1} h^2$ and selects that part of the parameter space of Eqs. (25) and (26) that satisfies the constraint of Eq. (3) as well as the LEP and Tevatron bounds on SUSY masses. One then calculates the event rate R for this allowed part of the parameter space. The solid lines in Figs. 5 and 6 show the maximum and minimum event rates for $\mu<0$ and $\mu>0$ as a function of A_t/m_0 for a Pb detector as one lets the remaining parameters vary over the allowed parameter space. (The relevant parts of these graphs are for the regions where $R_{\rm max} \geqslant 0.01$.) As can be seen from the previous discussion, the largest event rates occur for the largest allowed values of $\tan\beta$ and for the smallest values of $m_{\tilde{g}}$. [The sharp peaks and dips in the $R_{\rm max}$ curves arise from the fact that a small value of $m_{\tilde{g}}$ implies by Eq. (13) a small $m_{\tilde{W}_1}$. If this parameter point also satisfies the LEP cut that $m_{\tilde{W}_1} > 45$ GeV it is allowed and gives rise to a large event rate. Otherwise it is excluded.] The Pb detector is generally considerably more sensitive than the CaF_2 detector since its nuclear mass is considerably larger increasing the $R_{\rm SI}$ contribution [as seen from Eqs. (29) and (30)].

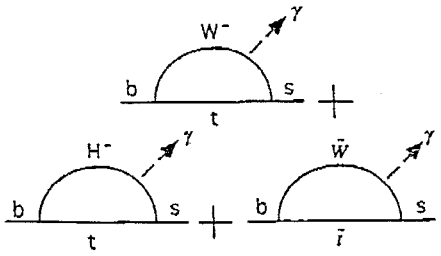

FIG. 4. Diagrams contributing to $b \to s+\gamma$ decay at W mass scale.

The solid lines in Figs. 5 and 6 also show that the parameter space is bounded in A_t with most of the allowed region occurring for $A_t > 0$. This phenomenon is due mainly to the fact that the t quark mass is large and hence close to its Landau pole. As one approaches the Landau pole, the light stop mass, $m_{\tilde{t}_1}$ obeys [20]

$$m_{\tilde{t}_1}^2 = -\frac{1}{3}\frac{A_R^2}{D_0} + m_{\tilde{t}_1}^2(\mathrm{NP}), \tag{34}$$

where

$$A_R \cong A_t - 0.613 m_{\tilde{g}}; \quad D_0 \cong 0.164[(m_t^f)^2 - (m_t)^2]/M_W^2. \tag{35}$$

$m_t^f \cong 197 \sin\beta$ is the fixed point mass, and $m_{\tilde{t}_1}^2(\mathrm{NP})$ is a relatively smooth nonpole contribution. For A_R^2 sufficiently large, the $\tilde{t}_1$ becomes tachyonic, eliminating such parameter points from the parameter space. One expects then a lower bound on A_t for $A_t < 0$, and similarly an upper bound for $A_t > 0$ (as we are requiring $m_{\tilde{g}} < 1$ TeV), with the domain of positive A_t being larger than for the negative A_t since cancelation in A_R between the A_t and $m_{\tilde{g}}$ term can occur in the former case. One finds, in fact, including correctly the nonpole part in Eq. (34), that for $m_t \simeq 170$ GeV

$$-0.6 \lesssim A_t/m_0 \lesssim 5.5. \tag{36}$$

Thus the high mass of the t quark eliminates a large amount of the SUSY parameter space.

V. CONSTRAINTS FROM $b \to s+\gamma$ DECAY

The $b \to s+\gamma$ decay is a sensitive test for new physics, since it is a flavor changing neutral current (FCNC) process. Thus the Standard Model and new physics loops enter at the same order. This is explicitly exhibited in Fig. 4. where the basic diagrams for the decay at scale $\mu \approx M_W$ are given for SUSY models. The W-t loop is common with the standard model, while the other loops are the additional supersymmetric contributions. The measured CLEO branching ratio for $B \to X_s+\gamma$ is [5]

$$\mathcal{B}(B \to X_s\gamma) = (2.32 \pm 0.5 \pm 0.29 \pm 0.32) \times 10^{-4} \tag{37}$$

or combining all errors in quadrature one has $\mathcal{B}(B\to X_s\gamma)\cong(2.32\pm0.66)\times10^{-4}$. This result represents an additional limitation on the allowed SUSY parameter space, and we discuss in this section the effect the CLEO data has on dark matter detection event rates.

In the spectator approximation, the B meson decay can be related to the b quark decay. It is convenient, to define the quantity R as

$$\frac{\mathcal{B}(B\to X_x\gamma)}{\mathcal{B}(B\to X_c e\overline{\nu_e})}\cong\frac{\Gamma(b\to s+\gamma)}{\Gamma(b\to c+e+\overline{\nu_e})}\equiv R. \tag{38}$$

[A Cahibbe-Kobayashi-Mashawa (CKM) and $(m_b)^5$ factor, which has large errors, cancels out in R.] Here $\mathcal{B}(B\to X_c e\overline{\nu_e})=(10.7\pm0.5)\%$. The diagrams of Fig. 4 can be described by an effective Hamiltonian [31]

$$H_{\rm eff}=V_{tb}V_{ts}^*\frac{G_F}{\sqrt{2}}C_7(M_W)Q_7, \tag{39}$$

where $Q_7=(e/24\pi^2)m_b\overline{s_L}\sigma^{\mu\nu}b_R F_{\mu\nu}$. Here $F_{\mu\nu}$ is the electromagnetic field strength and m_b is the b-quark mass. One must use the renormalization group equations to go from scale $\mu=M_W$ to $\mu\simeq m_b$ where the decay occurs. To leading order (LO) in QCD corrections, R is then calculated to be [31]

$$R=\left|\frac{V_{tb}V_{ts}^*}{V_{cb}}\right|^2\frac{6\alpha}{\pi I(z)}\,|C_7^{\rm eff}(m_b)|^2, \tag{40}$$

where $I(z)=1-8z^2+8z^6-z^8-24z^4\ln z$ is a phase space factor $(z=m_c/m_b)$ and

$$C_7^{\rm eff}(m_b)=\eta^{16/25}C_7(M_W)+\frac{8}{3}(\eta^{14/23}-\eta^{16/23})C_8(M_W)+C_2(M_W). \tag{41}$$

Here $Q_8=(g_3/16\pi^2)m_b\overline{s_R}\sigma^{\mu\nu}T^A b_L G^A_{\mu\nu}$, where T^A and $G^A_{\mu\nu}$ are the gluon generators and field strengths and C_2 represents operator mixing with the four-quark operators.

The QCD corrections are large for this process and the next to leading order corrections (NLO) are needed to obtain an accurate theoretical prediction. At present, however, not all the NLO terms have been calculated. Thus the theoretical analysis has an estimated error of about $\pm30\%$ with a standard model (SM) prediction of $\mathcal{B}[B\to X_s\gamma]\cong(2.9\pm0.8)\times10^{-4}$ for $m_t=174$ GeV [32]. The H^--t SUSY diagram of Fig. 4 adds constructively to the SM amplitude while the $\widetilde{W}-\widetilde{t}$ loop may enter constructively or destructively with the SM model amplitude. Since the central value of the CLEO data of Eq. (37) already lies about 1 std. below the central value of the SM results, the current data cannot tolerate a large amount of constructive interference with SUSY amplitudes. Thus, in spite of the large errors in the current data, the $b\to s+\gamma$ decay produces a significant constraint on the SUSY parameter space.

As seen from Eqs. (14), radiative breaking generally implies $m_{H^\pm}$ is large, suppressing its contribution to the $b\to s+\gamma$ decay. The $\widetilde{t}-\widetilde{W}$ diagram can become large, however, when $m_{\widetilde{t}_1}$ and $m_{\widetilde{W}_1}$ are small. The $\widetilde{t}$ (mass)^2 matrix reads

$$\begin{pmatrix} m^2_{\widetilde{t}_L} & m_t(A_t-\mu\cot\beta)\\ m_t(A_t-\mu\cot\beta) & m^2_{\widetilde{t}_R}\end{pmatrix}, \tag{42}$$

where expressions for $m^2_{\widetilde{t}_L}$, $m^2_{\widetilde{t}_R}$ are given in [20]. The light $\widetilde{t}$ eigenvalue is

$$m^2_{\widetilde{t}_1}=\frac{1}{2}(m^2_{\widetilde{t}_L}+m^2_{\widetilde{t}_R})-\left[\frac{1}{4}(m^2_{\widetilde{t}_L}-m^2_{\widetilde{t}_R})^2+m_t^2(A_t-\mu\cot\beta)^2\right]^{1/2}. \tag{43}$$

One has that $m^2_{\widetilde{t}_i}$ can become small if A_t is negative due to the Landau pole in Eqs. (34) and (35). Further when A_t and μ have the same sign the theoretical prediction for $B(b\to s+\gamma)$ will become large if also $m_{\widetilde{W}_1}$ is small, while the SUSY effect on $B(b\to s+\gamma)$ will be small for A_t and μ having opposite sign (or $m_{\widetilde{W}_1}$ becoming large). This can be seen explicitly to be the case from detailed computer calculations given in [33].

Equation (36) shows that the major part of the parameter space has $A_t>0$, and so the $b\to s+\gamma$ decay is expected to influence mostly the $\mu>0$ branch. One may quantify this by requiring that the theoretical rate for $B(b\to s+\gamma)$ be within the 95% C.L. bounds of the experimental value. One finds then that for $\mu>0$ one is restricted to the region

$$-0.25<A_t/m_0<0.5,\quad \mu>0; \tag{44}$$

i.e., about 40% of the parameter space of Eq. (36) is eliminated by the $b\to s+\gamma$ data. In addition, sections of the parameter space with small $m_{\tilde{g}}$ are eliminated for $A_t<0$, $\mu<0$ and for $0<A_t\leq0.5$, $\mu>0$.

The effects of the above restrictions are shown in Fig. 5 ($\mu<0$) and Fig. 6 ($\mu>0$). In Fig. 5 one sees that event rates are reduced in the small domain of $A_t<0$ (as the low $m_{\widetilde{W}_1}$ part of the parameter space is eliminated), but not significantly modified over the remainder of the parameter space where $A_t>0$, since here μ and A_t have opposite signs. Figure 6 shows that the only remaining part of the parameter space is the narrow band of $A_t<0.5$, and all of the parameter space with $A_t>0.5$ (where μ and A_t have the same sign) is eliminated. Thus the major effect of the $b\to s+\gamma$ data is to eliminate regions of parameter space, rather than reduce expected event rates. As can be seen from Figs. 5 and 6, there still remain regions of parameter space with large event rates. (This is to be contrasted with the results stated in [18].)

VI. VARYING THE BOUNDS ON $\Omega_{\widetilde{Z}_1}h^2$

The analysis considered above was done within the framework of the bounds of Eq. (3) on $\Omega_{\widetilde{Z}_1}h^2$. We consider now the effect of varying these bounds. We first note that the $\widetilde{Z}_1$ annihilation cross section in the early universe arising from the diagrams of Fig. 1 is a decreasing function of $m_{\widetilde{Z}_1}$. Alternately, from the scaling relations Eq. (13), one

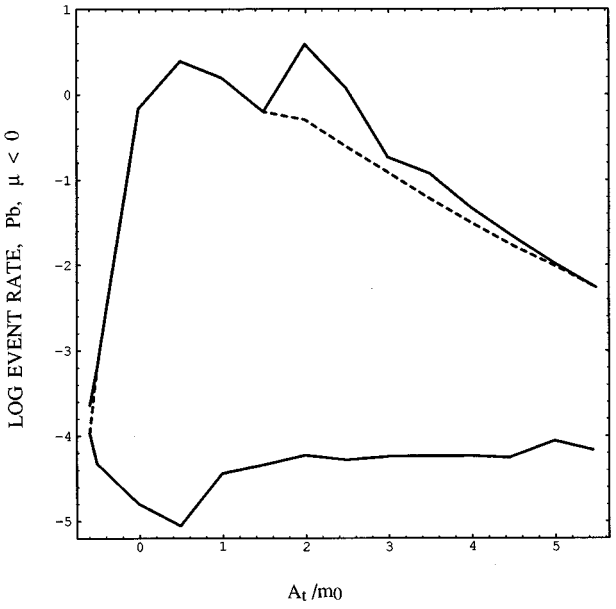

FIG. 5. Maximum and minimum event rates for Pb detector vs A_t/m_0 without $b\to s+\gamma$ constraint (solid) and with $b\to s+\gamma$ constraint (dashed) at 95% C.L. for $\mu<0$. Other parameters are varied over the range of Eqs. (25) and (26) with $m_t=168$ GeV. (The minimum event rates are unaffected by the $b\to s+\gamma$ constraint.)

may say then that $\Omega_{\tilde{Z}_1}h^2$ increases as $m_{\tilde{g}}$ increases. On the other hand, we saw in Sec. IV that the event rate R is a decreasing function of $m_{\tilde{g}}$. We are interested in this paper in the region $R\geqslant 0.01$ events/kg day which will be accessible experimentally in the forseeable future. This bound on R then puts an upper bound on $m_{\tilde{g}}$. The largest allowed value of $m_{\tilde{g}}$ occurs for the largest value of $\tan\beta$ and smallest value of m_0 [which by Eqs. (25) and (26) we are taking as $\tan\beta\leqslant 20$, $m_0\geqslant 100$ GeV], since R increases with $\tan\beta$ and decreases with m_0. One finds then for the parameter space defined by Eqs. (25) and (26) that for $\mu<0$ one has [34]

$$m_{\tilde{g}}\lesssim 650\ \text{GeV}\quad \text{for } R\geqslant 0.01,\ \ \mu<0. \tag{45}$$

For $\mu>0$, $m_{\tilde{g}}$ can rise to (700–750) GeV. However, this occurs for $A_t>0$, and as discussed in Sec. V, this region of the parameter space is eliminated by the $b\to s+\gamma$ decay data,

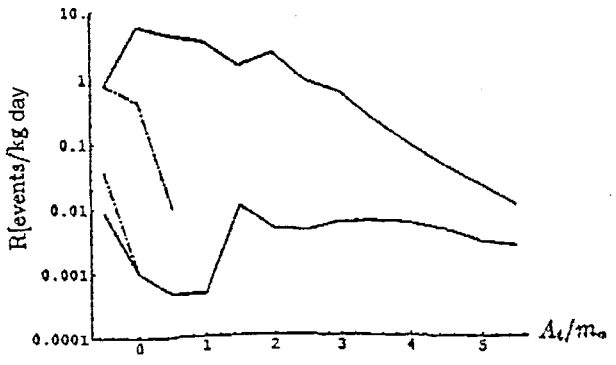

FIG. 6. Same as Fig. 5 for $\mu>0$. The parameter space with the $b\to s+\gamma$ constraint terminates for $A_t/m_0>0.5$.

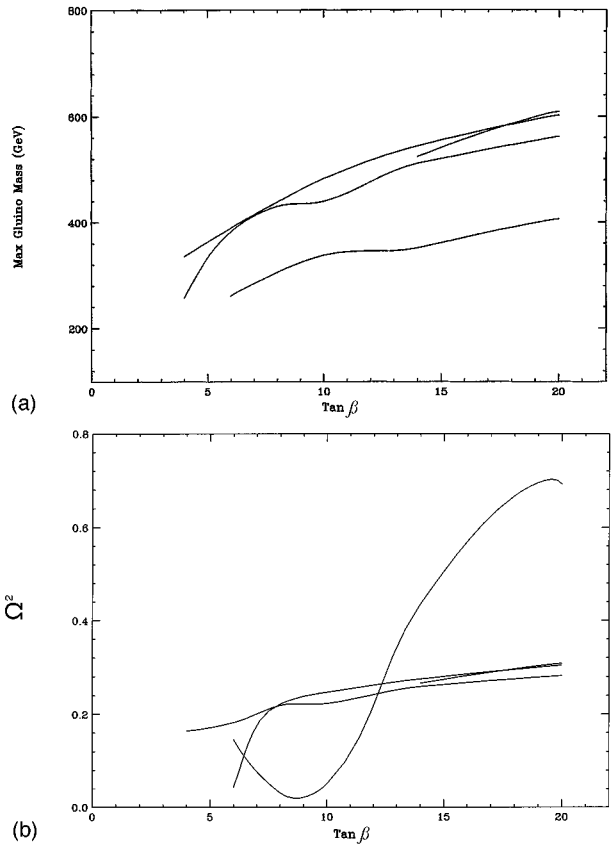

FIG. 7. Maximum value of $m_{\tilde{g}}$ (a) and the value of $\Omega_{\tilde{Z}_1}h^2$ at this $m_{\tilde{g}}$ (b) as a function of $\tan\beta$ for $\mu<0$ for domain $R>0.01$ events/kg day for Pb detector as other parameters are varied over range of Eqs. (25) and (26) with $m_t=168$ GeV. The curves are labeled by values of $A_t/m_0=0,2,3,4$ in ascending order of their end points on the right-hand side of (a), and $A_t/m_0=3,2,4,0$ in ascending order of their end point on the right-hand side for (b).

and so Eq. (45) represents the true upper bound on $m_{\tilde{g}}$ for dark matter that can be detected with current designs of detectors.

A detailed inspection of the full parameter space shows that the limitation $R<0.01$ implies then that the early universe annihilation channels $\tilde{Z}_1\tilde{Z}_1\to hh,Zh$ are closed. The channel $\tilde{Z}_1\tilde{Z}_1\to WW,ZZ$ is almost always closed, and the small regions in parameter space which allow this annihilation are very close to threshold and hence highly suppressed. Hence, one need not consider the vector meson channels in the analysis of $\Omega_{\tilde{Z}_1}h^2$ given in Sec. IV.

The behavior of $\Omega_{\tilde{Z}_1}h^2$ and R as a function of $m_{\tilde{g}}$ also shows that the bound $R\geqslant 0.01$ implies that $m_{\tilde{g}}\leqslant 650$ GeV. This is exhibited in Fig. 7(a). One sees, as shown in Fig. 7(b), that $\Omega_{\tilde{Z}_1}h^2<0.3$ when $R\geqslant 0.01$ at these maximum values of $m_{\tilde{g}}$ (except when A_t/m_0 is small and $\tan\beta$ is large). Thus in this domain, the results obtained above are not sensitive to the precise upper bound in Eq. (3). (The exceptional region of large Ωh^2 can occur when m_0 is large (reducing the relic annihilation rate) with a sufficiently large $\tan\beta$ to maintain $R>0.01$.) If one were to lower the upper bound below $\Omega_{\tilde{Z}_1}h^2=0.3$, then the upper bound on $m_{\tilde{g}}$ is further reduced. This is shown in Fig. 8, where it is seen that if $\Omega_{\tilde{Z}_1}h^2<0.2$, then $m_{\tilde{g}}<400$ GeV, which would make the

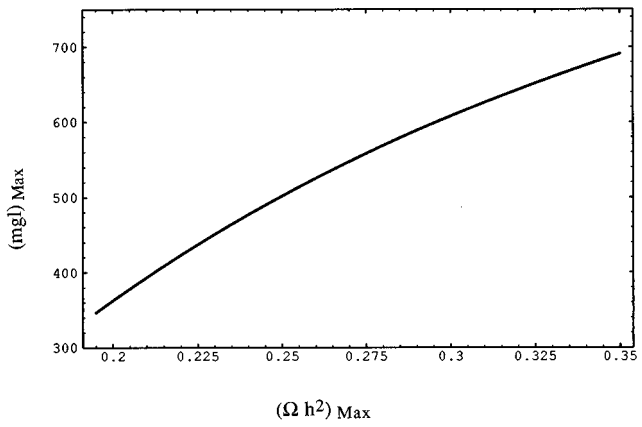

FIG. 8. Maximum value of $m_{\tilde{g}}$ as a function of the upper bound on $\Omega_{\tilde{Z}_1}h^2$ for $\mu<0$ for $\tan\beta=6$, $A_t/m_0=0.5$. (Results are insensitive to the values of $\tan\beta$ and A_t.)

gluino accessible to the proposed high luminosity upgrade of the Tevatron. We note that in both the inflationary scenario with a cold-hot dark matter mixture or the scenario with cold dark matter and a cosmological constant, low values of $\Omega_{\tilde{Z}_1}h^2$ are preferred. This follows from the fact that in the former case one needs a small value of h (i.e., $h\simeq 0.5$ so that the age of universe be consistent with the estimated age of globular clusters) in the latter case because $\Omega_{\tilde{Z}_1}$ is small (i.e., $\Omega_{\tilde{Z}_1}\simeq 0.2-0.4$ since the majority of the matter of the universe is in the cosmological constant).

We now turn to the question of sensitivity of results to the lower bound on $\Omega_{\tilde{Z}_1}h^2$. As discussed above, low $\Omega_{\tilde{Z}_1}h^2$ arises when $m_{\tilde{g}}$ is small, which is also the domain of parameter space where R can be large. Also, as discussed in Sec. IV, the peaks and dips of $R_{\max}$ in the solid lines in Figs. 5 and 6 arise from whether or not the LEP bound $m_{\tilde{W}_1}>45$ GeV can be satisfied. Figures 9 and 10 exhibit the effect on the maximum event rates for Pb and CaF_2 detectors when the bound $\Omega_{\tilde{Z}_1}h^2>0.10$ is raised to $\Omega_{\tilde{Z}_1}h^2>0.15$. One sees that the sharp peaks get reduced, but otherwise the results are qualitatively unchanged. There still remains, however, a sizable amount of parameter space where R exceeds 0.01.

VII. CONCLUSIONS

We have examined in this paper the direct detection possibility of $\tilde{Z}_1$ cold dark matter within the framework of the minimal supergravity model (MSGM) for the parameter space defined by Eqs. (25) and (26), and for relic densities $\Omega_{\tilde{Z}_1}h^2$ in the range given by Eq. (3). [Equation (3) encompasses the range one would expect from inflationary cosmology for either the cold-hot dark matter scenario or the cold dark matter plus cosmological constant possibility.] One further limits the parameter space so that experimental bounds on SUSY masses are obeyed. Two new pieces of data, the t quark mass and the $b\to s+\gamma$ branching ratio, have greatly constrained the SUSY parameter space. Thus the fact that m_t is large (i.e., close to its quasi infrared fixed point) limits the domain of A_t to be mostly positive, while the experimental $b\to s+\gamma$ decay rate limits the parameter space to be mostly

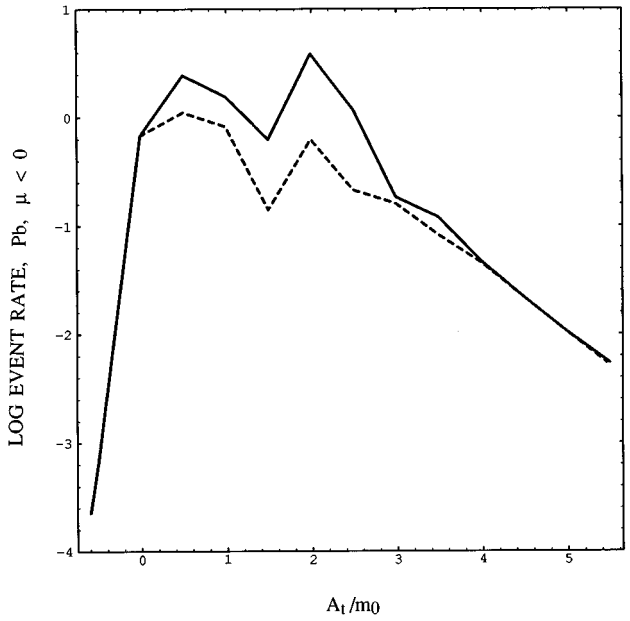

FIG. 9. Maximum event rates for Pb detector as a function of A_t/m_0 for $\mu<0$ for $\Omega_{\tilde{Z}_1}h^2>0.10$ (solid) and $\Omega_{\tilde{Z}_1}h^2>0.15$ (dashed). Other parameters are varied over the range of Eqs. (25) and (26) with $m_t=168$ GeV. (The $b\to s+\gamma$ decay constraint is not here imposed.)

where A_t and μ have the opposite sign. Thus the majority (though not all) of the allowed parameter space is in the region where $A_t>0$ and $\mu<0$.

Physical quantities in the MSGM depend on four SUSY parameters, m_0, $m_{\tilde{g}}$, A_t, $\tan\beta$, and the sign of μ. Thus a

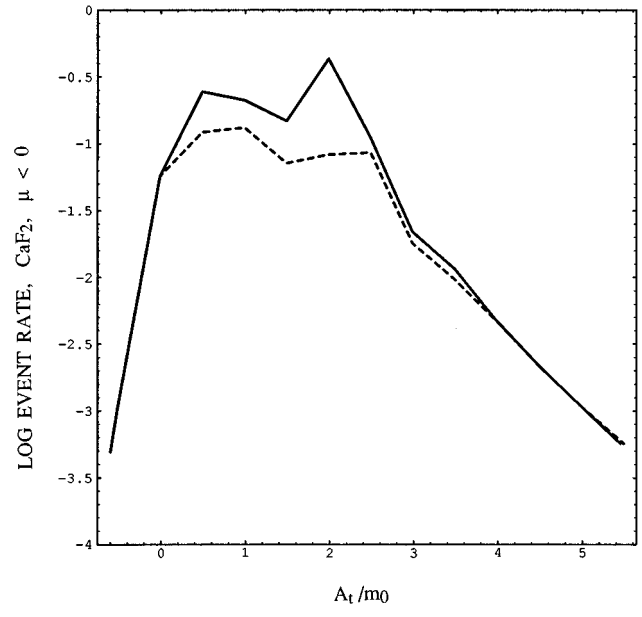

FIG. 10. Maximum event rates for CaF_2 detector as a function of A_t/m_0 for $\mu<0$ for $\Omega_{\tilde{Z}_1}h^2>0.10$ (solid) and $\Omega_{\tilde{Z}_1}h^2>0.15$ (dashed). Other parameters are varied over the range of Eqs. (25) and (26) with $m_t=168$ GeV. (The $b\to s+\gamma$ decay constraint is not here imposed.)

general quantity has a complex behavior as one varies over the full parameter space. Radiative breaking, however, plays a central role in MSGM predictions and allows one to understand analytically the qualitative behavior of the event rate for the detection of $\tilde{Z}_1$ dark matter. Approximate analytic expressions were obtained in Sec. III for the content of the $\tilde{Z}_1$ showing that the $\tilde{Z}_1$ was mostly bino, but with a non-negligible amount of Higgsino. One can see from this that the spin independent (coherent) contribution generally dominates R (and hence the most sensitive detectors are those with the heaviest nuclei) and that R decreases with m_0 and $m_{\tilde{g}}$ and increases with $\tan\beta$.

Current dark matter detectors hope to obtain a sensitivity of $R>0.01$ events/kg day in the forseeable future. As seen here, such a sensitivity will allow the exploration of a sizable amount of the SUSY parameter space, though there will still remain large sections that fall below this bound. The domain $R>0.01$ corresponds to $m_{\tilde{g}}\lesssim 650$ GeV and is insensitive to the choice of upper bound on $\Omega_{\tilde{Z}_1}h^2$ of Eq. (3) for most of the parameter space provided $(\Omega_{\tilde{Z}_1}h^2)_{\max}\gtrsim 0.3$, and only mildly sensitive to the lower bound of Eq. (3). Thus dark matter could only be expected to be seen by current detector designs if the gluino is not too heavy.

ACKNOWLEDGMENTS

We wish to thank Manuel Drees for pointing out a sign error on the μ term in Eq. (42) in the first version of this paper. This research was supported in part by NSF Grants No. PHY-9411543 and No. PHY-19306906 and at the Institute of Theoretical Physics at Santa Barbara by Grant No. PHY94-07194.

APPENDIX

In $N=1$ supergravity there are three possible candidates for the lightest supersymmetric particle (LSP). These are the $\tilde{Z}_1$, the $\tilde{\nu}$, and the $\tilde{e}_R$. We discuss here the region of parameter space where the $\tilde{Z}_1$ is the LSP. The basic requirement for this is then that

$$m_{\tilde{e}_R}>m_{\tilde{Z}_1};\quad m_{\tilde{\nu}}>m_{\tilde{Z}_1}. \tag{A1}$$

In addition one has the LEP constraint that

$$m_{\tilde{Z}_1}\gtrsim 20\ \text{GeV}. \tag{A2}$$

The requirement that the $\tilde{e}_R$ be heavier than $\tilde{Z}_1$ is an experimental constraint as otherwise a charged LSP would have already been discovered. We will see that in fact this condition is obeyed for almost the entire parameter space. The region where the $\tilde{\nu}$ is the LSP will also be seen to be very small.

The $\tilde{e}_R$ and $\tilde{\nu}$ masses can be expressed in terms of the basic MSGM parameters as [4]

$$m^2_{\tilde{e}_R}=m_0^2+\tilde{\alpha}_G\ \tfrac{6}{5}\ f_1 m_{1/2}^2-\sin^2\theta_W M_Z^2\cos 2\beta, \tag{A3}$$

$$m^2_{\tilde{\nu}}=m_0^2+\overline{\alpha_G}[\tfrac{3}{2}\ f_2+\tfrac{3}{10}\ f_1]m_{1/2}^2+\tfrac{1}{2}\ M_Z^2\cos 2\beta, \tag{A4}$$

where the form factors $f_i(t)$ are defined as

$$f_i(t)=t(2+\beta_i t)/(1+\beta_i t)^2, \tag{A5}$$

where $t=2\ln(M_G/Q)$ and $\beta_i=\tilde{\alpha}_G(\frac{33}{5},1,-3)$ are the U(1)$\times$SU(2)$\times$SU(3) β functions with $\tilde{\alpha}_G=\alpha_G/4\pi$. In the following we use $\alpha_G=1/24$, $M_G=2\times 10^{16}$ GeV, $Q=M_Z$. One finds then $f_1\cong 38.1$, $f_2\cong 99.0$, $f_3\cong 772.0$. In order to analytically illustrate the results, we will perform the remainder of the calculation in the scaling limit of Eqs. (13) and (14). (A more accurate numerical calculation gives results close to the analytic ones.) One can then relate $m_{1/2}$ to the $\tilde{Z}_1$ mass by

$$m_{\tilde{Z}_1}\cong\tilde{m}_1=(\alpha_1/\alpha_G)m_{1/2} \tag{A6}$$

or $m_{1/2}\cong 2.45 m_{\tilde{Z}_1}$. Equations (A3) and (A4) then become

$$m^2_{\tilde{e}_R}\cong m_0^2+0.912 m^2_{\tilde{Z}_1}-\sin^2\theta_W M_Z^2\cos 2\beta, \tag{A7}$$

$$m^2_{\tilde{\nu}}\cong m_0^2+3.19 m^2_{\tilde{Z}_1}+\tfrac{1}{2}\ M_Z^2\cos 2\beta. \tag{A8}$$

The requirement that the $\tilde{e}_R$ not be the LSP then becomes an upper bound on $m_{\tilde{Z}_1}$:

$$m_{\tilde{Z}_1}<11.4[m_0^2+\sin^2\theta_W M_Z^2(-\cos 2\beta)]. \tag{A9}$$

Similarly, the condition that the $\tilde{\nu}$ is heavier than the $\tilde{Z}_1$ becomes a lower bound on $m_{\tilde{Z}_1}$:

$$m^2_{\tilde{Z}_1}>0.456[-m_0^2+\tfrac{1}{2}\ M_Z^2(-\cos 2\beta)]. \tag{A10}$$

Equations (A9), (A10), and (A2) are three inequalities constraining the parameters $m_{\tilde{Z}_1}$, m_0, and $\tan\beta$. In addition we have the fine tuning constraints of m_0, $m_{\tilde{g}}<1$ TeV.

In the scaling limit then Eq. (A9) implies, for $m_{\tilde{g}}=1$ TeV,

$$m_0>41.9\quad \text{for } \tan\beta=1;\quad m_0\gtrsim 0\quad \text{for } \tan\beta\gtrsim 4.7, \tag{A11}$$

with corresponding smaller lower bounds on m_0 for smaller values of $m_{\tilde{g}}$. Thus for almost the entire parameter space the MSGM predicts that the $\tilde{e}_R$ is not the LSP.

Turning to the $\tilde{\nu}$ constraint, we see that the right-hand side of Eq. (A10) falls below the LEP bound Eq. (A2) (and hence becomes irrelevant) when

$$m_0^2>\tfrac{1}{2}\ M_Z^2(-\cos 2\beta)-(20)^2/0.456 \tag{A12}$$

and hence

$$m_0\gtrsim 0\quad \text{for } \tan\beta<1.24;\quad m_0>57.3\ \text{GeV}\quad \text{for } \tan\beta\gtrsim 1. \tag{A13}$$

Alternately for all $\tan\beta$, Eq. (A10) is satisfied for all m_0 if $m_{\tilde{Z}_1}>43.6$ GeV (or $m_{\tilde{g}}>308$ GeV). Thus the $\tilde{\nu}$ is predicted to be heavier than the $\tilde{Z}_1$ for all but a very small portion of the parameter space.

[1] E. Gates, G. Gyuk, and M. Turner, Phys. Rev. Lett. **74**, 3724 (1995).

[2] L. M. Krauss and M. Turner, Report No. CWRU-P6-95-FERMILAB-Pub-95/063-A, astro-ph/9504003 (unpublished).

[3] A. H. Chamseddine, R. Arnowitt, and P. Nath, Phys. Rev. Lett **29**, 970 (1982). For reviews, see *Applied N=1 Supergravity* (World Scientific, Singapore, 1984); H. P. Nilles, Phys. Rep. **110**, 1 (1984); R. Arnowitt and P. Nath, in *Particles and Fields*, Proceedings of the 7th Summer School Jorge Andre Swieca, Sao Paulo, Brazil, 1993, edited by O.J.P. Eboli and V.O. Rivelles (World Scientific, Singapore, 1994).

[4] K. Inoue *et al.*, Prog. Theor. Phys. **68**, 927 (1982); L. Ibañez and G. G. Ross, Phys. Lett. **110B**, 227 (1982); L. Avarez-Gaumé, J. Polchinski, and M. B. Wise, Nucl. Phys. **B221**, 495 (1983); J. Ellis, J. Hagelin, D. V. Nanopoulos, and K. Tamvakis, Phys. Lett. **125B**, 2275 (1983); L. E. Ibañez and C. Lopez, Nucl. Phys. **B233**, 545 (1984); L. E. Ibañez, C. Lopez, and C. Muños, *ibid.* **B256**, 218 (1985).

[5] CLEO Collaboration, M. S. Alam *et al.*, Phys. Rev. Lett. **74**, 2885 (1995).

[6] CDF Collaboration, F. Abe *et al.*, Phys. Rev. Lett. **74**, 2626 (1995); D0 Collaboration, S. Abachi *et al.*, *ibid.* **74**, 2632 (1995).

[7] J. Ellis and R. Flores, Phys. Lett. B **263**, 259 (1991); **300**, 175 (1993); Nucl. Phys. **B400**, 25 (1993).

[8] K. Greist, Phys. Rev. Lett. **61**, 666 (1988).

[9] A. Bottino *et al.*, Astron. Part. Phys. **1**, 61 (1992); **2**, 77 (1994).

[10] M. Drees and M. Nojiri, Phys. Rev. D **48**, 3483 (1993).

[11] G. Kane, C. Kolda, L. Roszkowski, and J. Wells, Phys. Rev. D **49**, 6173 (1994); E. Diehl, G. Kane, C. Kolda, and J. Wells, *ibid.* **52**, 4223 (1995).

[12] R. Arnowitt and P. Nath, Mod. Phys. Lett. A **10**, 1257 (1995).

[13] P. Nath and R. Arnowitt, Phys. Lett. B **336**, 395 (1994); Phys. Rev. Lett. **74**, 4592 (1995).

[14] K. Greist and D. Seckel, Phys. Rev. D **43**, 3191 (1991); P. Gondolo and G. Gelmini, Nucl. Phys. **B360**, 145 (1991).

[15] R. Arnowitt and P. Nath, Phys. Lett. B **299**, 58 (1993); **303**, 403(E) (1993); P. Nath and R. Arnowitt, Phys. Rev. Lett. **70**, 3696 (1993). After completion of this paper there has appeared an analysis by H. Baer and M. Brhlick, Phys. Rev. D **53**, 597 (1996), which implements numerically the computation of the relic density without using a power series expansion in velocity near an *s*-channel resonance. The thermal averaging of this analysis is equivalent to ours.

[16] M. Kamionkowski, Phys. Rev. D **44**, 3021 (1991).

[17] M. Kamionkowski, L. Krauss, and M. Ressel, Report No. IASSN-HEP-94/14-CWRU-P3-94 (unpublished).

[18] F. Borzumati, M. Drees, and M. Nojiri, Phys. Rev. D **51**, 341 (1995).

[19] P. Langacker, talk at SUSY 95, Palaiseau, France, 1995 (unpublished).

[20] P. Nath, J. Wu, and R. Arnowitt, Phys. Rev. D **52**, 4169 (1995).

[21] R. Arnowitt and P. Nath, Phys. Rev. Lett. **69**, 725 (1992); P. Nath and R. Arnowitt, Phys. Lett. B **289**, 368 (1992).

[22] As will be discussed in Sec. VI, for $R>0.01$ events/kg day, the annihilation channels into vector bosons and Higgs bosons are effectively closed.

[23] B. W. Lee and S. Weinberg, Phys. Rev. Lett. **39**, 165 (1977); D. A. Dicus, E. Kolb, and V. Teplitz, *ibid.* **50**, 1419 (1983); H. Goldberg, *ibid.* **50**, 1419 (1983); J. Ellis, J. S. Hagelin, D. V. Nanopoulos, and M. Srednicki, Nucl. Phys. **B238**, 453 (1984).

[24] M. W. Goodman and E. Witten, Phys. Rev. D **31**, 3059 (1993); K. Greist, *ibid.* **38**, 2357 (1988); **39**, 3802 (E) (1989); R. Barbieri, M. Frigeni, and G. F. Giudice, Nucl. Phys. **B313**, 725 (1989); M. Srednicki and R. Watkins, Phys. Lett. B **225**, 140 (1989).

[25] A factor of 4 has been included in Eqs. (29) and (30) to account for the Majorana nature of the $\tilde{Z}_1$, in accord with Ref. [10].

[26] J. F. Gunion, H. E. Haber, G. Kane, and S. Dawson, *The Higgs Hunter's Guide* (Addison-Wesley, Redwood City, CA 1990).

[27] H. Haber and R. Hempfling, Phys. Rev. Lett. **60**, 1815 (1991); Phys. Rev. D **48**, 4280 (1993); J. Ellis, G. Ridolfi, and F. Zwirner, Phys. Lett. B **262**, 477 (1991).

[28] EMC Collaboration, J. Ashman *et al.*, Nucl. Phys. **B328**, 1 (1989); A. Manohar and R. Jaffe, *ibid.* **B337**, 509 (1990).

[29] SMC Collaboration, D. Adams *et al.*, Phys. Lett. B **329**, 399 (1994); E143 Collaboration, R. Arnold *et al.*, in *Intersections of Particle and Nuclear Physics*, Proceedings of the Conference, St. Petersburg, Florida, 1994, edited by W.T.H. van Oers, AIP Conf. Proc. No. 338 (AIP, New York, 1995).

[30] T. P. Cheng, Phys. Rev. D **38**, 2869 (1989); J. Gasser, H. Leutwyler, and M. E. Saino, Phys. Lett. B **253**, 252 (1991).

[31] S. Bertolini, F. Borzumati, and A. Masiero, Phys. Rev. Lett. **59**, 180 (1987); B. Grinstein, R. Springer, and M. B. Wise, Nucl. Phys. **B339**, 269 (1990); S. Bertolini, F. Borzumati, A. Masiero, and G. Ridolfi, *ibid.* **B353**, 591 (1991); R. Barbieri and G. Giudice, Phys. Lett. B **309**, 86 (1993); M. Misiak, *ibid.* **269**, 161 (1991); Nucl. Phys. **B393**, 23 (1993).

[32] A J. Buras, M. Misiak, M. Münz, and S. Pokorski, Nucl. Phys. **B424**, 374 (1994); M. Ciuchini, E. Franco, G. Martinelli, L. Reina, and L. Silvestrini, Phys. Lett. B **316**, 127 (1993).

[33] J. Wu, P. Nath, and R. Arnowitt, Phys. Rev. D **51**, 1371 (1994).

[34] We use here the value of *R* for a Pb detector, since this detector is most sensitive as it has the highest mass nuclei.